Dalton Transactions

ROYAL SOCIETY OF CHEMISTRY

PAPER

View Article Online
View Journal | View Issue

Check for updates

Cite this: *Dalton Trans.*, 2025, **54**, 10935

Relating structure, composition, and spin crossover properties in Hofmann complexes†

Matthew G. Robb [a,b] and Hanna L. B. Boström [a,b]*

Received 20th May 2025,
Accepted 13th June 2025

DOI: 10.1039/d5dt01192b

rsc.li/dalton

Spin crossover (SCO) is attractive for applications within *e.g.* sensing or solid-state cooling, but controlling the properties is extremely challenging. Hofmann complexes, with formula $FeL_xM(CN)_4{\cdot}G$ (L = organic ligand, G = guest) are archetypical SCO-active coordination polymers, associated with strong cooperativity and large guest sensitivity. This manuscript presents a metastudy of over 300 Hofmann complexes, analysing crystal structures with symmetry-mode analysis with the aim of clarifying the link between structure, composition, and SCO behaviour. The distortion landscape is dominated by shifts of the inorganic layers and tilts perpendicular to the stacking direction. The transition temperatures are typically maximised for 3D Hofmann complexes with M = Pd or Pt and few (or no) symmetry-lowering structural distortions. Our results are relevant for the rational design of spin-crossover active materials with a wealth of applications.

Open Access Article. Published on 13 June 2025. Downloaded on 1/22/2026 6:47:46 AM.
This article is licensed under a Creative Commons Attribution 3.0 Unported Licence.

1 Introduction

Spin crossover (SCO)—reversible switching between the high and low spin states (HS/LS) of a transition metal—is fascinating for inorganic chemists and materials scientists alike. While theoretically possible in any transition metal with electron configuration d^4–d^7, it is predominantly observed in Fe^{II} ions coordinated by N-bearing ligands.[1] Despite this compositional limitation, a large diversity of SCO materials exist due to the multitude of possible organic ligands and crystal structures. Thermal switching of the SCO is the most commonly studied,[2] and is characterised by $T_{1/2}$, the temperature where 50% of the Fe^{II} ions have undergone the transition, and hysteresis width $\Delta T_{1/2}$. SCO can also be induced by external pressure,[3] guest absorption,[4,5] and various forms of radiation.[6–8]

The many stimuli and the strong coupling between spin states and optical/magnetic properties lead to a wealth of SCO-based applications,[9] including actuators,[10] sensors,[11] and memory devices.[12] Recently, SCO has also emerged as an intriguing mechanism for barocaloric cooling, *i.e.* pressure-driven refrigeration based on a solid–solid phase transition.[13–15] This circumvents the issues of harmful gases exploited in current cooling technologies.[16] The specific application stipulates the ideal properties of the SCO transitions. For example, memory devices require abrupt transitions with large hysteresis loops,[12] barocaloric applications rely on abrupt transitions *without* hysteresis,[17] and both gradual and abrupt transitions can be exploited for sensors.[18] Common to most applications, however, is the need for a near-ambient $T_{1/2}$, as most devices should be operational at room temperature. The varying requirements and strong pool of useful applications motivate the development of design rules for spin crossover.

As $T_{1/2}$ is a function of the crystal field strength around the Fe^{II} ion, crystal engineering of SCO properties might be thought to be straightforward. Nonetheless, this is a profound challenge, as most SCO systems are incredibly sensitive to both chemical and structural changes, where the latter can be difficult to control. While methods have been developed to predict the $T_{1/2}$ of SCO complexes prior to synthesis—*e.g.* Hammett parameters[19] or calculated $\delta(^{15}N)$ values[20]—these are typically performed for solution-phase compounds. The solid state, on the contrary, is more complicated due to the potential for polymorphism and solvatomorphism. For example, the α-polymorph of a particular co-crystal shows SCO, but the β-polymorph does not.[21] Even isotopic labelling can give small, but noticeable changes to $T_{1/2}$ and the hysteresis width.[22] While this sensitivity increases the scope for property optimisation, it adds to the challenge of controlling the spin transition.

For most switching applications, abrupt transitions are preferred, which is favoured by strong cooperativity between the metal centres. Cooperativity is generally enhanced if the SCO-active metal centres are covalently linked, which motivates the study of SCO-active coordination polymers.[1] Perhaps the most prolific family is the Hofmann complexes, $FeL_xM(CN)_4{\cdot}G$,

[a]*Department of Chemistry, Stockholm University, Svante Arrhenius väg 16C, SE-106 91 Stockholm, Sweden. E-mail: hanna.bostrom@mmk.su.se*
[b]*Wallenberg Initiative Materials Science for Sustainability, Department of Chemistry, Stockholm University, SE-114 18 Stockholm, Sweden*

† Electronic supplementary information (ESI) available. See DOI: https://doi.org/10.1039/d5dt01192b

Open Access Article. Published on 13 June 2025. Downloaded on 1/22/2026 6:47:46 AM.
This article is licensed under a Creative Commons Attribution 3.0 Unported Licence.

where L is an N-bearing ligand, $x \in \{1,2\}$, M∈{Ni, Pd, Pt} and G is a guest molecule [Fig. 1].[23,24] Their strong cooperativity, structural diversity through the choice of the organic ligand, and potential porosity places Hofmann complexes at the forefront of the field of SCO-active coordination polymers.

Hofmann complexes can form either 2D or 3D covalent networks, as dictated by the denticity of the ligand L. For monodentate L (*e.g.* pyridine), $x = 2$ and the structure forms planes of square $FeM(CN)_4$ units capped by L. These layers are typically offset relative to each other, so that the ligands interdigitate, facilitated by van der Waals or aromatic interactions [Fig. 1(a)].[27] Such structures are generally referred to as 2D Hofmann complexes. For bidentate L (*e.g.* pyrazine), the layers are pillared by Fe–L–Fe bonds, giving 3D metal–organic frameworks with open metal M-sites [Fig. 1(b)].[27] 3D Hofmann complexes are often porous, which enables sensing of suitable guest molecules.[28] Due to the variety of organic linkers—in turn dictating whether a 2D or 3D topology forms—and the tunability of the M-site, the scope for crystal engineering is substantial.

In addition to the different topologies, Hofmann complexes can adopt a range of symmetries. This is largely thanks to the flexibility and symmetry of the organic ligands, but distortions of the $FeM(CN)_4$ layers are generally involved as well. These distortions—which can be very large[29]—are sometimes referred to as undulation/rippling,[30–32] and typically involve rotations or translations of metal polyhedra. In that sense, they can be compared to the rigid-unit modes pervasive in perovskites, including molecular perovskites—a family known for its flexibility and many degrees of freedom.[33,34] Hofmann complexes constitute layered versions of Prussian blue analogues and their layered structure opens up for new types of rigid-unit modes compared to topologically cubic perovskites. Given the sensitivity of SCO properties to structural changes, these distortions are likely to interplay with the SCO behaviour, yet are rarely discussed in detail.

In this manuscript, we present a metastudy of the Hofmann complexes with FeN_6 coordination present in the Cambridge Structural Database (version 5.46), giving a database with 321 compounds, with 89 different linkers. The article commences with a description of the methods used, followed by a classication and analysis of the structural distortions. Subsequently, the link between composition, structure and SCO properties is discussed. For example, we demonstrate that Ni-based Hofmann complexes are considerably less likely to show SCO than systems where M = Pd or Pt, and a low number of symmetry-lowering distortions and 3D topology appear to correlate with high $T_{1/2}$ values.

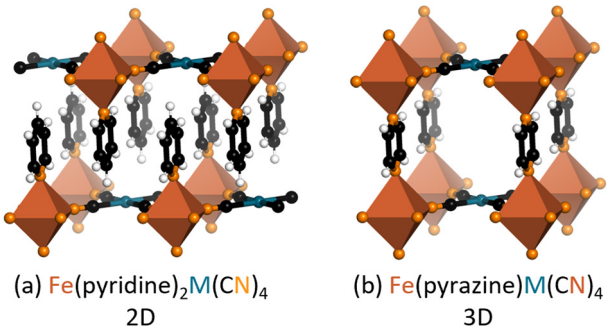

Fig. 1 (a) 2D $Fe(pyridine)_2 M(CN)_4$,[25] and (b) 3D $Fe(pyrazine)M(CN)_4$.[26] Fe is shown in brown, N in orange, C in black, H in white, and M in dark blue. Linker disorder has been removed for clarity.

2 Methods

Full experimental details are given in the ESI,† and this section provides a brief overview of symmetry-mode analysis. Symmetry-mode analysis treats a low-symmetry, distorted "child" (or hettotype) crystal structure as derived from a high-symmetry "parent" (or aristotype) structure, with the addition of one or more modes of distortions—similar to frozen vibrational normal modes. For example, the low-temperature *R3m* structure of $BaTiO_3$ can be described as the parent $Pm\bar{3}m$ cubic perovskite with displacements of the Ti^{IV} ion towards the unit cell corner, *i.e.* [111].[35,36] In symmetry-mode language, the distortions are represented by irreducible representations (irreps), denoted by Miller–Love notation.[37] The displacement of the Ti^{IV} ions in $BaTiO_3$ transforms as Γ_4^- with the order parameter direction (a,a,a), which denotes the displacement direction.[36] Note that the irrep labels depend on the parent space group and unit cell setting, so can not be compared across structures with different parents.

Γ_4^- is the so-called primary order parameter in the $BaTiO_3$ example, meaning that it is solely responsible for the observed *R3m* symmetry.[36] Only one primary order parameter is present here, but several possible sets of primary order parameters may exist in other cases. Normally, there will also be secondary order parameters—distortions that become allowed by the symmetry lowering of the primary order parameter. In the present example, the only secondary order parameter is Γ_5^+, which corresponds to lattice strain and deformation of the TiO_6 units. Often, a large number of primary order parameters correlates with more secondary order parameters. However, not all these modes will be of sufficiently large magnitude to be noticeable in the crystal structure.

Symmetry-mode analysis, using the freely available ISODISTORT software,[38] can identify the distortion modes present in a child structure, relative to a given parent. Information about the relative magnitude of the modes and the possible primary and secondary order parameters is available. This can be used to pinpoint the primary order parameters in complex structures with a multitude of active distortions—for example following a phase transition—which can be difficult to perform by eye. Moreover, symmetry-mode analysis facilitates structural comparisons between child structures with the same parent, which fosters an understanding the distortion preferences of a particular family of compounds.[39–41] It is also helpful in the search for special symmetries, *e.g.* polarity *via* hybrid improper ferroelectricity.[42–44]

This journal is © The Royal Society of Chemistry 2025

Open Access Article. Published on 13 June 2025. Downloaded on 1/22/2026 6:47:46 AM.
This article is licensed under a Creative Commons Attribution 3.0 Unported Licence.

3 Results

3.1 Structure

Symmetry-mode analysis, implemented in the software ISODISTORT,[38] can be used to analyse topologically identical structures [see Methods for a description]. This section discusses the structures of the 205 Hofmann complexes present in the CSD from a symmetry-mode point of view, grouped by classes of rigid-unit distortions. A comprehensive treatment is beyond the scope of this study, yet the most frequent zone-centre and zone-boundary distortions are included. The distortions discussed below are summarised in Tables S1–S3 and Fig. S3–S5.†

3.1.1 Layer slides and shear modes. The $FeM(CN)_4$ layers in Hofmann complexes can translate relative to each other, irrespective of whether the layers are covalently linked (3D) or not (2D). We denote this degree of freedom "layer shift".[40] If no layer shift is present, the Fe (M) atoms are located directly above the Fe (M) atoms in adjacent layers, giving parent symmetry *P*4/*mmm* [Fig. 2(a)]. This is akin to a double version of Dion–Jacobson phases[45,46] and the Fe–L vectors are collinear in the absence of further distortions. Hence, it is unsurprising that *P*4/*mmm* symmetry predominantly occurs for rigid bidentate ligands, such as pyrazine[47] or bis(4-pyridyl)acetylene,[48] or small monodentate ligands (NH_3 [49]) where steric clashing is minimal.

A layer shift of $(\frac{1}{2},0,0)$ or $(0,\frac{1}{2},0)$ gives symmetry *Ammm* (≡*Cmmm*) [Fig. 2(b)]. The non-standard space group setting ensures that *c* remains perpendicular to the inorganic layers, for consistency with the *P*4/*mmm* parent. The *Ammm* structure is equivalent to the well-known Ruddlesden–Popper perovskite phases.[50] Both Fe and M are directly above the $Fe[M(CN)_4]$ windows in the nearby layers; hence the ligands interdigitate for 2D complexes. Consequently, *Ammm* symmetry is common for rigid monodentate ligands with the possibility of π-stacking, including pyridine,[51] 2-(4-pyridyl)benzimidazole,[52] and the isomers pyridazine[53] and pyrimidine.[29] 3D Hofmann complexes never adopt *Ammm* symmetry, as a result of the layer shift.

Finally, a layer offset of $(\frac{1}{2},\frac{1}{2},0)$ relative to the *P*4/*mmm* structure gives parent symmetry *I*4/*mmm*, where the Fe atoms are directly above the M atoms and *vice versa* [Fig. 2]. This also resembles a Dion–Jacobson phase.[45,46] Unlike the two previous discussed parent structures, the undistorted *I*4/*mmm* parent is not yet experimentally observed. While some Hofmann complexes adopt structures close to *I*4/*mmm* parent,[54,55] the Fe–M–Fe stacking along *c* is not perfect. Hence, these structures can be treated as subgroups of *Ammm*, and this is the case in this manuscript.

Non half-integer values of layer shifts are also possible, which is described by the irreps Z_5^- (*P*4/*mmm*) and Y_2^-/Y_3^- (*Ammm*) [Fig. 3(a)]. The lower symmetry of the *Ammm* parent means that there will be two irreps associated with distortions propagating perpendicular to *c*. Neither distortion is particularly common and they only occur in combination with other primary order parameters. Out of these, Y_2^- is the most frequent and together with other modes (Z_4^-) gives the symmetry *Pnma*. This is seen in *e.g.* Hofmann complexes based on pyrimidine derivatives[31,56] and some compounds with long and complex ligands.[57,58] Hofmann complexes close to the *I*4/*mmm* parent show large values of Y_2^-.[55]

The most common means to non-special values of layer shifts is a shear distortion of the unit cell. This couples to octahedral tilts—which will be discussed in the subsequent section—and can thus be seen as a mixed shift–tilt mode [Fig. 3(a)]. For the parent *P*4/*mmm* phase, the relevant shear mode transforms as Γ_5^+ and gives either $P\bar{1}$, *P*2/*m*, or *C*2/*m* symmetry, depending on the shear (*i.e.* order parameter) direction. These child structures are all well represented amongst Hofmann complexes, in particular the former two.[29,59–61] Uniaxial shear, giving *P*2/*m* symmetry, exclusively occurs in 3D complexes. For *Ammm*, the equivalent irreps are Γ_2^+ and Γ_3^+, where the latter is common and gives the space group *C*2/*m*. About half of the compiled Hofmann complexes feature shear modes, regardless of parent, making it the most common distortions. This highlights the (unsurprising) importance of layer shifts as a flexibility mechanism in Hofmann complexes.

To summarise, the majority of Hofmann complexes display a shift of the inorganic metal–cyanide layers relative to the *P*4/*mmm* parent. A continuum of layer shift values are possible and certain special half-integer values give rise to a different parent structure (*Ammm*). Given the high prevalence of layer shifts, Fe (M) are rarely stacked directly above the Fe (M) ions in the adjacent layers. This preference likely results from the need to avoid unfavourable head-on interactions of the ligands for 2D complexes, and instead allow sideways π-stacking of aromatic moieties.

3.1.2 Tilting. (Octahedral) tilting is a well-known distortion in perovskites,[62] and—as the name suggests—involves rotations of rigid octahedra whilst preserving the topology. In

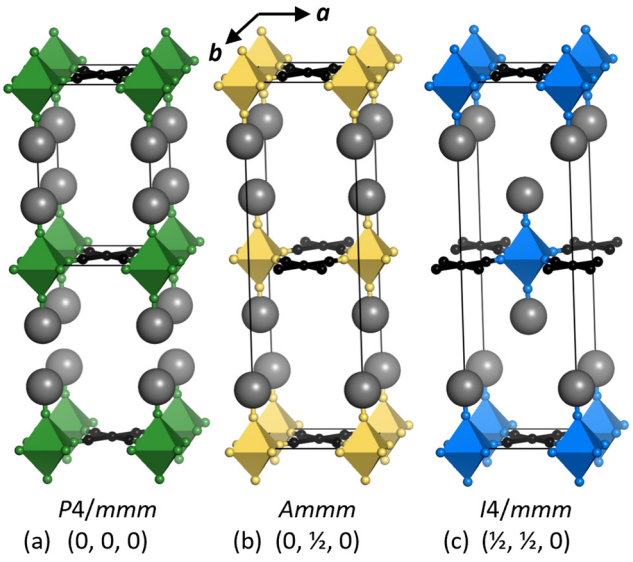

Fig. 2 The three parent structures for Hofmann complexes: (a) *P*4/*mmm*, (b) *Ammm*, and (c) *I*4/*mmm*, distinguished by the relative layer shift of the middle layer, as indicated. FeN_6 is shown in green/yellow/blue, MC_4 in black and a generic organic ligand indicated by a grey sphere. The unit cell is highlighted in black.

Open Access Article. Published on 13 June 2025. Downloaded on 1/22/2026 6:47:46 AM.
This article is licensed under a Creative Commons Attribution 3.0 Unported Licence.

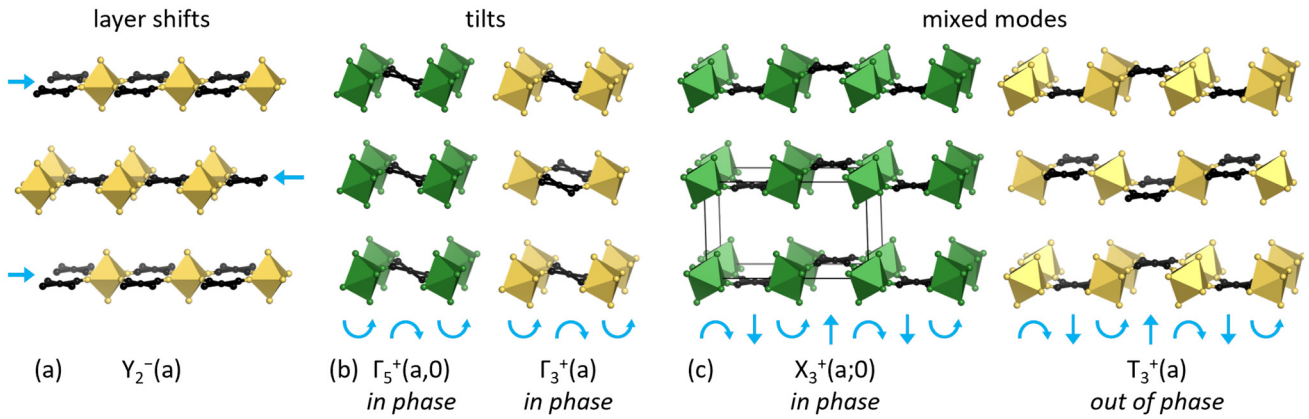

Fig. 3 Examples of rigid-unit distortions in Hofmann complexes: (a) layer shifts, (b) tilts, and (c) mixed tilt–shift modes. The irrep, order parameter direction and correlation along *c* (vertical, in phase/out of phase) are given for each distortion. Structures with the *P*4/*mmm* and *Ammm* parents are shown in green and yellow, respectively.

perovskite oxides, these distortions often underlie phase transitions,[39,63] and interplay with the electronic properties.[64] As will be shown, tilt modes are common in Hofmann complexes, though some rotating units are $M(CN)_4$ squares rather than octahedra.

A number of parameters are needed to describe a particular tilt mode. First, the propagation axis indicates the direction of the rotation. In layered systems, tilts can propagate along the stacking direction *c*—sometimes called rotations, rather than tilt—or along a perpendicular axis *a*/*b*. Second, in-phase (out-of-phase) tilts refer to columns of octahedra along the propagation axis rotating in the same (opposite) directions.[62] Layer shifts, *e.g.* in the *Ammm* parent, blur the concept of phase for distortions along *c*, as the octahedra/squares no longer form columns. We use "in-phase" when like units—FeN_6 or $M(CN)_4$—tilt in the same sense. Finally, one can distinguish conventional from unconventional tilts, which relates to the correlations perpendicular to the tilt axis.[65] Yet, as cyanide frameworks predominantly tilt conventionally,[66] this is ignored here. For tilts along *a* or *b*, the correlation along *c* still matters, as the tilts of individual layers are decoupled. Altogether, all the possible combinations (axes, phases, *c* correlations) yield a plethora of tilt modes.

Out of the multitude of tilt distortions theoretically accessible for Hofmann complexes, only a fraction is experimentally observed. In particular, octahedral rotations polarised along *c* are surprisingly rare. Out-of-phase rotations are not present at all, and while some compounds display in-phase modes—transforming as Γ_3^+ (*P*4/*mmm*) and Γ_4^+ (*Ammm*)—the magnitudes are barely noticeable. Two compounds undergo phase transitions from *Imma* to *I*2/*c* (≡*C*2/*c*),[67–69] associated with the Γ_4^+ irrep, but this appears to be driven by ligand ordering rather than by distortions of the inorganic layers. Accordingly, rotations along *c* are not critical to Hofmann complexes.

In contrast to rotations along *c*, tilts along *a*/*b* relative to the parent phase are ubiquitous. Shear modes—Γ_5^+ (*P*4/*mmm*) and Γ_2^+/Γ_3^+ (*Ammm*)—were mentioned in the context of layer shifts, and appear in about half of the studied complexes. These distortions couple to out-of-phase tilts along *a*/*b* with in-phase correlations along the *c* direction. The corresponding modes with out-of-phase *c* correlations transform as Z_5^+ (*P*4/*mmm*) and Y_2^+/Y_3^+ (*Ammm*). Y_3^+ exclusively occurs if the linker lacks rotatable bonds, such as halogenated pyridines and pyrazines.[70,71] A noteworthy example is 2D $Fe(pyrazine)_2Ni(CN)_4$, which is one of the few examples of a Hofmann complex with a Ni–N interaction (2.8 Å), giving pseudo-octahedral coordination of Ni. At ambient conditions, Y_3^+ is the sole primary order parameter and upon cooling, an additional Y_2^+ tilt changes the symmetry from *Pmna* to $P2_1/c$, albeit with a very small magnitude.[32] This highlights the possibility of tilt-induced phase transitions, similar to perovskites.

The key message from this subsection is that tilts along *a*/*b* are prevalent in Hofmann complexes. The coupling to shear for some of the Γ-modes is notable, as it implies a layer shift, which offsets the ligands for 2D complexes. In contrast, tilts along *c* are rare.

3.1.3 Shifts and mixed modes. Layer shifts are a subset of the so-called columnar shifts,[72] which involve correlated displacements of columns/sheets of octahedra. This degree of freedom is unique to systems with polyatomic linkers, as these allow translation without octahedral distortions.[72] In Hofmann complexes, a large number of shift periodicities are possible, by virtue of the layered structure. Translations of inorganic layers were discussed above, and can be described as layer shifts polarised along *a* or *b*. In contrast, shifts polarised along *c* are essentially not experimentally observed in Hofmann complexes.

The layered structure of Hofmann complexes allows for distortions comprising both tilts and shifts, where *e.g.* the $M(CN)_4$ squares shift along *c* and the FeN_6 octahedra tilt along a perpendicular axis—or *vice versa* [Fig. 3(c)]. These "mixed modes" have no counterpart in unlayered perovskites, yet are frequent in Hofmann complexes. The most common mixed mode involves displacement of $M(CN)_4$ units with tilting FeN_6

 This journal is © The Royal Society of Chemistry 2025

Open Access Article. Published on 13 June 2025. Downloaded on 1/22/2026 6:47:46 AM. This article is licensed under a Creative Commons Attribution 3.0 Unported Licence.

octahedra, which act as hinging points. If in phase along *c*, it transforms as X_3^+ (*P*4/*mmm* parent) [Fig. 3] and brings ligands bound to adjacent Fe^{II} ions close together. The proximity might explain why X_3^+ commonly coexists with the Γ_5^+ shear mode,[73–75] which offsets the layers, avoiding clashing ligands. Compounds with the X_3^+ mode typically contain flexible ligands with multiple rotatable bonds—*e.g. N*-cinnamalidene-4-amino-1,2,4-triazole[76] or bis(4-pyridyl)butadiyne[75]—which may also help to minimise unfavourable steric interactions. The equivalent distortion in *Ammm* is denoted by Z_3^+, but is rare.

The out-of-phase version of the mixed mode X_3^+ is denoted R_3^+ (*P*4/*mmm* parent). This results in four ligands pointing towards the centre of a cavity [Fig. 3(c)]. R_3^+ is rare and the known examples show weakly bent bidentate ligands with substantial disorder to avoid clashing ligands.[77,78] For the *Ammm* parent, the equivalent mode transforms as T_3^+ and is one of the most frequent distortions, occurring either as the single primary order parameter, giving *Imma* symmetry,[30,69] or be combined with other modes.[30,31] The layer shift in *Ammm* alleviates the risk for unfavourable steric interactions between the ligands. Like for X_3^+ in *P*4/*mmm*, compounds with T_3^+ often comprise long and complex ligands, but some Hofmann complexes with simple ligands—*e.g.* imidazolate[67] and triazolate[79]—also display this distortion.

The *Ammm* parent can harbour mixed modes with translation of the FeN_6 octahedra, described by Z_4^- and T_4^-. This is not observed in complexes with the *P*4/*mmm* parent. Z_4^- involves displacements of FeN_6 units and tilts of $M(CN)_4$, in phase along *c*, leading to the space group *Cmcm*. This appears in compounds with *e.g.* small ligands based on monosubstituted pyridine and pyrimidine.[31,56] The out-of-phase version of Z_4^-—described by T_4^-—is only known for compounds with L = 4-ethyl-disulfanylpyridine.[80] Overall, mixed modes with $M(CN)_4$ shifts are favoured over translating FeN_6 units.

To summarise, pure columnar shifts are rare in Hofmann complexes, whereas mixed tilt–shift modes are exceedingly common, in particular T_3^+ (*Ammm*). Since mixed modes with tilting FeN_6 units bring ligands close together, it is unsurprising that these modes often coexist with layer shifts—either *via* the *Ammm* parent or shear modes for *P*4/*mmm*.

3.2 Structure–property relationships

Crystal engineering involves deriving relationships between the composition, structure, and the properties of interest. In Hofmann complexes, the main compositional degrees of freedom are the metal M, the linker L, and solvation. The structure can be described by the symmetry, topology—dictated by the linker denticity—and the active distortion modes, as outlined above. The SCO behaviour is quantified by the number of transition steps, the transition temperature $T_{1/2}$, and the hysteresis width $\Delta T_{1/2}$. Thus, SCO inactivity can be seen as 0 steps and $T_{1/2}$ = 0. Following a description of the number of SCO transition steps, this section outlines the role played by each compositional and structural degree of freedom on the SCO properties.

About 85% of the collated Hofmann complexes show spin crossover, which can occur in one or more steps [Fig. 4(a)–(c)]. One-step transitions are the most prevalent and appear in 60% of the complexes. About 15% remain HS at all temperatures and only ~5% display SCO transitions with more than 2 steps. In general, a larger number of steps appears to correlate with lower $\Delta T_{1/2}$ and $T_{1/2}$ [Fig. S6†]. As SCO in practice only occurs in a limited temperature range, a high $\Delta T_{1/2}$ decreases the number of steps that can be accommodated. There is no obvious correlation between the $T_{1/2}$ and $\Delta T_{1/2}$ values of the individual steps in a multistep transition [Fig. S6†]. Looking at completeness, the majority of incomplete one-step transitions show $T_{1/2}$ values in the range 100–200 K and all transitions with $T_{1/2}$ > 300 K are complete [Fig. S7†]. As multistep transitions have incomplete transitions by definition, discussions of completeness are less meaningful here.

Starting with the effect of the M-site metal, Hofmann complexes with Ni generally distinguish themselves relative to systems where M = Pd or Pt. Only ~65% of all Ni-based complexes show SCO, whereas the corresponding figure is ~90% for Pd and Pt [Fig. 4(a)]. Consequently, replacing Pt/Pd with Ni can sometimes remove the SCO behaviour completely [Fig. S8†]. Ni-based Hofmann complexes also tend to show lower $T_{1/2}$ than those based on the heavier ions [Fig. 4(d) and Fig. S8†]. An interesting exception is Fe(pyrazine)$M(CN)_4$, which shows the reverse trend.[47] Though in general, Ni favours the HS state to a larger extent than systems with Pd or Pt.

Identifying suitable descriptors for the linker is less straightforward. However, the number of rotatable bonds [see section 1 in the ESI† for definition] can be seen as a crude quantification of the flexibility. A relatively large proportion (>70%) of the Hofmann complexes without SCO contains linkers with no rotatable bonds [Fig. 4(b)]—*e.g.* pyrazine, pyridine, and functionalised derivatives. The number of rotatable bonds correlates with $T_{1/2}$: $T_{1/2}$ > 300 K is only found if the linker has 0–1 rotatable bonds and all compounds with >2 rotatable bonds show $T_{1/2}$ values below 250 K [Fig. 4(e) and S9†]. As for the hysteresis, one might expect rigid frameworks—*i.e.* few rotatable bonds—to display higher cooperativity and thus larger $\Delta T_{1/2}$ values, but no strong trend is seen. In brief, linkers with large conformational flexibility generally favour the HS state.

Turning to the topology—stipulated by the linker denticity—the distribution of 2D and 3D frameworks across the number of transition steps is purely statistical [Fig. 4(d)]. The highest $T_{1/2}$ values are found in 3D frameworks [Fig. 4(h)], though this could reflect the inherent bias of the dataset. The compounds with $T_{1/2}$ > 298 K are based on three ligands only: pyrazine, bis(4-pyridyl)acetylene, and quinoxaline, with varying metals and solvation. A further implication of the topology is that 3D frameworks are often porous, and guest molecules can have a considerable impact on $T_{1/2}$.[28] The higher connectivity of 3D frameworks should increase the cooperativity and could therefore be expected to increase $\Delta T_{1/2}$,[81] but this is not reflected in the data.

Fig. 5 shows the $T_{1/2}$–$\Delta T_{1/2}$ phase space with selected primary order parameters highlighted [Fig. S10 and S11† show

Open Access Article. Published on 13 June 2025. Downloaded on 1/22/2026 6:47:46 AM.
This article is licensed under a Creative Commons Attribution 3.0 Unported Licence.

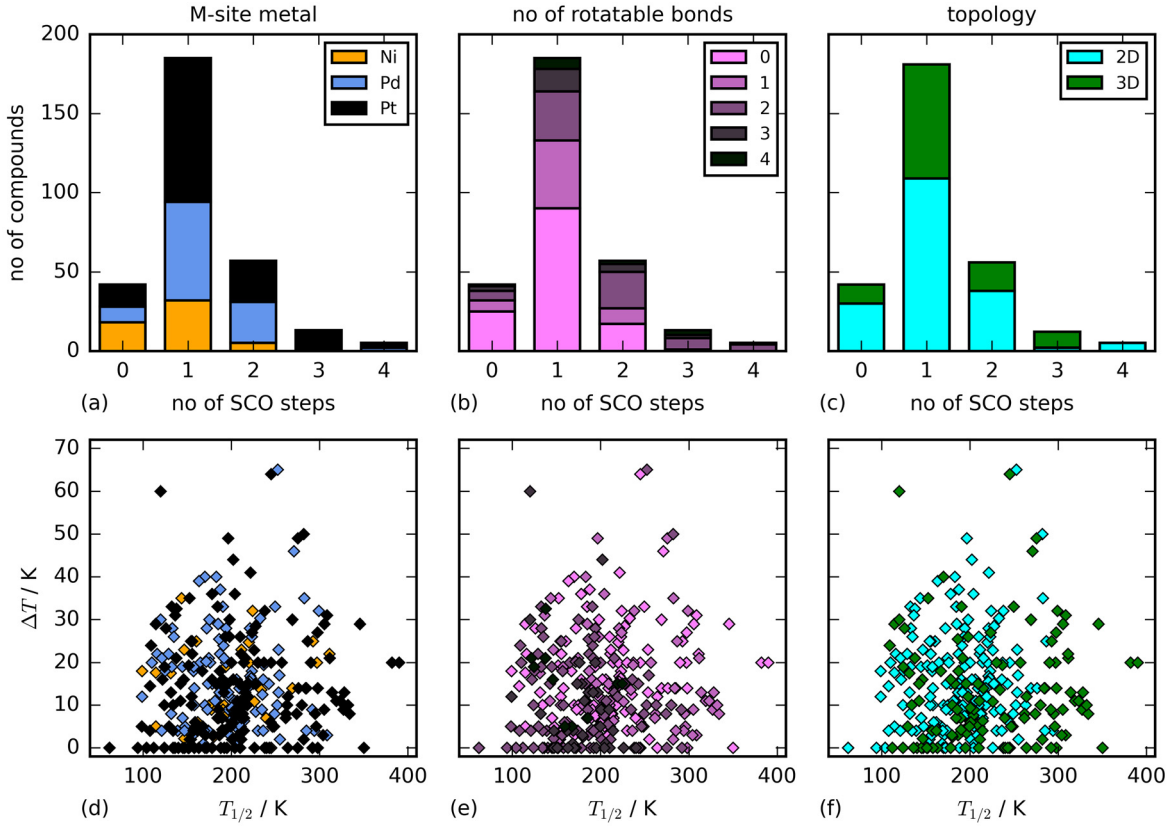

Fig. 4 The distribution of Hofmann complexes with SCO transitions with 0–4 steps (0 steps and $T_{1/2}$ = 0 indicate no SCO), coloured by (a) M-site metal, (b) the number of rotatable bonds, (c) the topology. The lower panels (d–f) show the $T_{1/2}$ and $\Delta T_{1/2}$ values, with the same colour scheme as in (a)–(c).

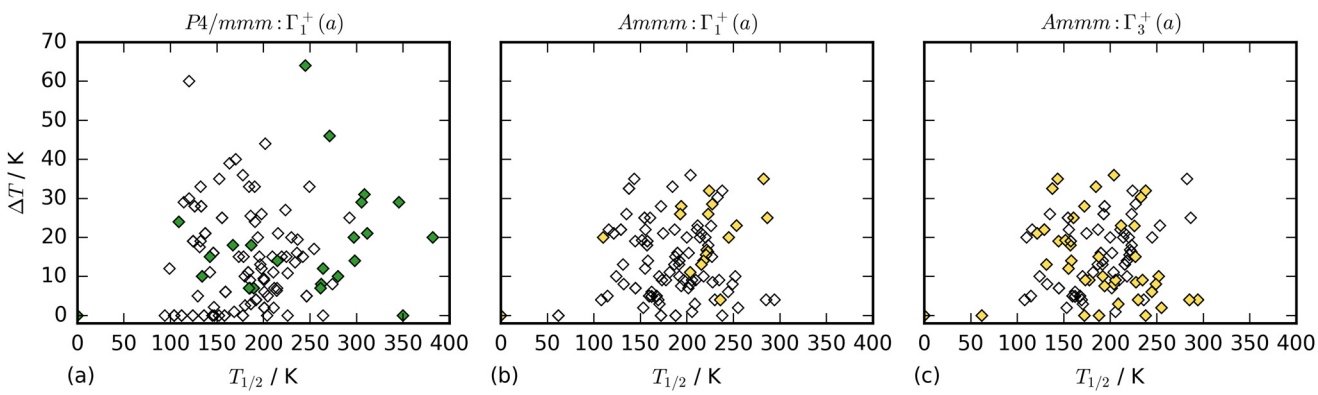

Fig. 5 The $T_{1/2}$–$\Delta T_{1/2}$ distribution of Hofmann complexes in the CSD, highlighting selected primary order parameters. (a) Hofmann complexes with the *P*4/*mmm* parent with Γ_1^+ as primary order parameter highlighted with filled green symbols. (b) and (c) show compounds with the *Ammm* parents and Γ_1^+ and Γ_3^+ highlighted in yellow, respectively.

a wider range of modes]. Γ_1^+ (*P*4/*mmm* parent) is the primary order parameter in the Hofmann complexes with the highest $T_{1/2}$ values, although it is not a sufficient condition for high transition temperatures. This irrep describes the totally symmetric representation, and so these compounds adopt the same symmetry as the parent *P*4/*mmm*. In other words, the absence of symmetry-lowering distortions is favourable for high $T_{1/2}$ values. For structures based on *Ammm*, the compounds with the highest $T_{1/2}$ values feature Γ_1^+ or Γ_3^+ as primary order parameters. The prevalence of Γ_1^+ in high-$T_{1/2}$ complexes implies that distortions of the inorganic framework lower the crystal field strength.

Finally, it is worth relating the composition and distortion modes (composition–structure relationships). This underpins

 This journal is © The Royal Society of Chemistry 2025

Open Access Article. Published on 13 June 2025. Downloaded on 1/22/2026 6:47:46 AM.
This article is licensed under a Creative Commons Attribution 3.0 Unported Licence.

the success of tilt engineering approaches used to construct polar symmetry in perovskites, by way of example.[82] For Hofmann complexes with the *P*4/*mmm* parent, linkers with 0 rotatable bonds (*i.e.* pyrazine) often adopt the aristotype *P*4/*mmm* symmetry. The corresponding trend is not seen for *Ammm*-based structures, where distortions are common even for rigid linkers. In other words, linkers without rotatable bonds are more likely to cause tilts and other distortions if a layer shift is active, as in the *Ammm* parent.

Moreover, the linker binding angle can determine the crystal structure of 3D complexes. The parent *P*4/*mmm* space group requires an angle of 180° between the terminal N atoms. Fe[2,5-bis(4-pyridyl)thiophene]Pt(CN)$_4$ shows a considerably lower binding angle of 133°, which induces the unusual R_3^+ distortion [Fig. 6(a)].[77] Likewise, the extremely large Z_4^- mode in Fe(pyrimidine)$_2$Ni(CN)$_4$ results from the interaction of pyrimidine with the Ni ion—giving a Ni–N distance of 2.4 Å—in addition to the Fe–N bond.[29] The binding angle of pyrimidine forces the framework to distort [Fig. 6(b)]. This illustrates how the linker can dictate the distortions of the inorganic layers and could provide a pathway towards crystal engineering.

The metal M exerts a smaller influence on the structure than the linker. This is to be expected, given that the variation in the ionic radii of the different metals is minor, in comparison with the wide variety of sizes and shapes accessible to the linker. There are a few compounds where the structure depends on M, *e.g.* the Pt and Pd analogues of Fe(3-chloropyridine)$_2$M(CN)$_4$ crystallise in *Pnc*2 or *Pmna* (depending on the temperature) and *C*2/*m*, respectively.[70] Yet, in the majority of cases, the structures of Hofmann complexes are invariant to the nature of the metal.[29,53,71,83]

4 Discussion

Hofmann complexes evidently display a range of displacive rigid-body distortions of the inorganic layers, similar to the topologically cubic (molecular) perovskites. In perovskites, tilt instabilities can be described by soft mode theory, and the onset of tilts is a key driving force for phase transitions. Phase transitions resulting from the condensation of rigid-unit distortions also appear in Hofmann complexes; typical modes include Γ_5^+ (*P*4/*mmm*)[84,85] and T_3^+ (*Ammm*).[86,87] However, sometimes the structural rearrangement required to undo a distortion mode would require substantial atomic displacements. For example, linker rotation would be needed for reversal of the distortion in Fe[2,5-bis(4-pyridyl)thiophene]Pt(CN)$_4$ in Fig. 6(a), which can be energetically costly, especially if the linkers are hydrogen bonded. Likewise, the energy barrier associated with reversal of the mixed tilt–shift mode in Fe(pyrimidine)$_2$ Ni(CN)$_4$ [Fig. 6(b)] will be high, as the Ni–N interaction would break. Consequently, the distortion modes in Hofmann complexes may be more likely to be static and not influenced by temperature, relative to perovskites. Similar behaviour is seen in thiocyanate-based molecular perovskites.[88]

In principle, a diverse set of accessible distortions increases the likelihood of hybrid improper ferroelectricity. This mechanism involves the coupling of two non-polar distortions to collectively lift inversion symmetry, giving a noncentrosymmetric —-and ideally polar—structure.[42–44] Hybrid improper ferroelectricity occurs when two modes with the same periodicity (irrep letter) but opposite sign are present, *e.g.* X_3^+ and X_2^-.[42] Perhaps surprisingly, polar symmetry is relatively rare in Hofmann complexes, though one example includes the *Pna*2$_1$ symmetry of Fe[*N*-(pyridin-4-yl)furan-2-carboxamide]$_2$Pd(CN)$_4$·H$_2$O·EtOH,[86] which is driven by the layer shift Y_2^- and the tilt Y_4^+.

Of all Hofmann complexes, those based on Ni often stand out in terms of the SCO properties. Ni favours the HS state, relative to Pd and Pt, which manifests in lower $T_{1/2}$ and a lower probability for SCO to occur. This likely stems from the higher electronegativity of Ni, which leads to withdrawal of electron density from the CN ligand. Hence, the σ-donating ability of the N atom is reduced, and the crystal field decreases, favouring high spin. The less favourable SCO properties induced by Ni might account for the low number of reported Ni-based compounds, compared to those based Pd and Pt. From a practical viewpoint, this is unfortunate, given its lower cost of Ni relative to the heavier metals. While Hofmann complexes are normally structurally invariant to the nature of M, the handful of compounds that display ligand–M interactions both contain Ni.[29,32] However, few such systems exist, and hence generalisation regarding the potential importance of M is difficult. As a final point, we note that there is little work carried out regarding solid M-site solutions, which might provide another path towards tunability.

Our numerical analysis is complicated by the complexities of defining unique compounds, and the risk of reporting bias. Different solvatomorphs, *i.e.* identical frameworks with different extents or types of guest molecules, are treated as distinct here, given that solvation often changes the SCO behaviour substantially.[28] Since some systems—such as Fe(pyrazine)Pt(CN)$_4$—have received disproportionately large attention due to their favourable properties, many solvatomorphs are reported. They are therefore overrepresented in our database,

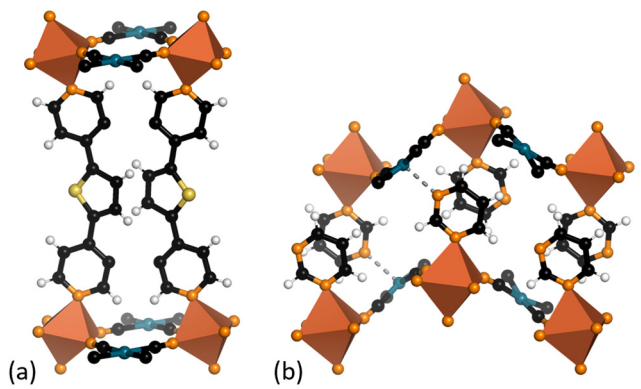

Fig. 6 Two Hofmann complexes with a clear link between the linker binding angle and the structural distortions. (a) Fe[2,5-bis(4-pyridyl)thiophene]Pt(CN)$_4$ [77] and (b) Fe(pyrimidine)$_2$Ni(CN)$_4$.[29] Fe is shown in brown, N in orange, C in black, H in white, S in yellow, and Pt/Ni in blue. The Ni–N interaction in (b) is shown by a dashed line.

Open Access Article. Published on 13 June 2025. Downloaded on 1/22/2026 6:47:46 AM.
This article is licensed under a Creative Commons Attribution 3.0 Unported Licence.

so to provide an alternative view, Fig. S12† reiterates Fig. 4 but only including desolvated frameworks. While the exact numbers differ, the overall trends are similar. Note that the exclusion of solvated complexes necessarily leads to an underrepresentation of 3D structures, since many naturally contain solvents from the synthesis. A further source of error is that compounds without SCO may be less likely to be published (reporting bias). Despite these caveats, the present analysis provides a useful overview of trends in the structure and SCO behaviour of Hofmann complexes.

Reproducibility is a cornerstone of science, and our database allows for comparison between nominally identical samples. For example, $T_{1/2}$ for the well-studied Fe(pyrazine)Pt(CN)$_4$·2H$_2$O is reported as both 230 K[47] and 274 K,[26] and reported $\Delta T_{1/2}$ values can also vary by ~10 K for the same complex.[87,89] A wide variety of reasons could cause this spread in values. Particle size influences the cooperativity, and accordingly the SCO properties,[90] yet is rarely reported. Solvation state is also critical,[28,91] though not necessarily easy to probe, as disordered solvent is challenging to locate crystallographically. It can also be difficult to distinguish between surface and pore water during thermogravimetric analysis (TGA). As for $\Delta T_{1/2}$, values measured by magnetometry depend on the heating rate,[92] which hampers comparisons. The above analysis also highlighted the overall difficulty to rationalise $\Delta T_{1/2}$ based on structural features. This reinforces the importance of proper structural and compositional characterisation, and highlights the difficulties associated with reproducibility in a field as sensitive as spin crossover.

A further aspect that might contribute to irreproducibility is the presence of defects and unnoticed disorder. Hofmann complexes—at least the 3D structures—are a subclass of metal–organic frameworks, where defects (often in the form of linker and node vacancies) are widespread.[93] Yet this is rarely discussed in Hofmann complexes. While the possibility of defects has been mentioned,[94,95] no studies have focused specifically on this, to the best of our knowledge. Likewise, investigations into the local structures of SCO complexes in general are scarce.[96] Crystal structures, as captured by a crystallographic information file (CIF), only describe the average structure, which may differ considerably from the "true" structure.[97] Given how sensitive SCO is to structural changes, defects and their (dis)order are likely to have critical implications for the functionality, and the field may benefit from future investigations in this regard.

5 Conclusion and outlook

This metastudy reports trends in crystal structure and spin crossover behaviour of Fe-containing Hofmann complexes, by analysing a database of 321 compounds reported in literature and crystallographic databases. As for the structure, Hofmann complexes display a range of displacive rigid-body distortions of the inorganic layers. While the layered structure and low symmetry give a large number of possible distortions, a relatively small subset of all theoretical modes is experimentally observed. Some of the most prevalent distortions include layer shifts and shear modes coupled to octahedral tilting; both of which serve to offset the inorganic layers. This allows for interdigitating linkers, which is important in 2D complexes. Modes comprising a mixture of tilts and shifts are particularly common, whereas there is a paucity of sole tilt and shift modes polarised along the stacking direction *c*. While it is difficult to generally predict the structure based on knowledge of the composition, the linker binding modes and flexibility can provide structural insights in favourable cases.

Turning to the SCO properties, one-step transitions dominate for all Hofmann complexes. Ni favours the HS state, which is reflected in both lower $T_{1/2}$ values for the Ni-based compounds and a lower frequency of SCO. For most applications, $T_{1/2} \sim 298$ K is desirable, which in general means striving to increase $T_{1/2}$. Our results show that $T_{1/2}$ is typically maximised for 3D frameworks with M = Pd or Pt and few (or no) symmetry-lowering structural distortions. One-step transitions are empirically found to give higher $T_{1/2}$ relative to multistep transitions. Neither guest inclusion nor longer linkers is a barrier to high $T_{1/2}$ values.[26,94] In contrast, incorporation of halides, particularly I, on the M-site gives some of the largest transition temperatures reported for Hofmann complexes.[98,99] However, neither of these criteria is a sufficient condition, and no single factor can dictate the SCO behaviour. In light of this, the recent developments in spin state prediction using machine learning[100,101] are intriguing. We note that group-theoretical descriptors—as used here—have been successfully used for the featurisation of machine learning models.[102]

There are many avenues for further study into the structure–property relationships in Hofmann complexes. For example, transition abruptness is outside the scope of this study, yet critical for applications. Moreover, there are a plethora of other possible descriptors of the linker—*e.g.* shape, size and H-bonding—that could be investigated. The linker is arguably the most obvious feature of a Hofmann complex, and so further in-depth studies of its influence will be welcome. Ultimately, the SCO behaviour is influenced by the electronic properties of the linker, which are difficult to infer from structural data. It is also noteworthy that the largest $T_{1/2}$ values are found in Hofmann complexes where halogen has been oxidatively added to the Pt open metal sites[98,99] and in spite of this strong effect, this does not appear to have been explored for compounds with other ligands than pyrazine.

To conclude, Hofmann complexes are fascinating materials with rich behaviour and despite the ostensibly simple structure, linking composition, structure and properties is not trivial. Clarification of the link between the structure and properties—as this article has endeavoured—will be valuable, given the growing potential applications of spin crossover.

Author contributions

MGR carried out the Conquest search, HLBB performed the symmetry-mode analysis, and the remaining analysis was per-

 This journal is © The Royal Society of Chemistry 2025

formed by both authors. The paper was written by HLBB and revised by MGR.

Conflicts of interest

There are no conflicts to declare.

Data availability

The data supporting this article have been included as part of the ESI.†

Acknowledgements

The authors acknowledge financial support from the Wallenberg Initiative Materials Science for Sustainability (WISE) funded by the Knut and Alice Wallenberg Foundation. HLBB acknowledges funding from the Swedish Research Council (V. R.) with grant number 2022-02984.

References

1 P. Gütlich, Y. Garcia and H. A. Goodwin, *Chem. Soc. Rev.*, 2000, **29**, 419–427.
2 D. J. Harding, P. Harding and W. Phonsri, *Coord. Chem. Rev.*, 2016, **313**, 38–61.
3 A. B. Gaspar, G. Molnár, A. Rotaru and H. J. Shepherd, *C. R. Chim.*, 2018, **21**, 1095–1120.
4 E. Resines-Urien, E. Fernandez-Bartolome, A. Martinez-Martinez, A. Gamonal, L. Piñeiro-López and J. S. Costa, *Chem. Soc. Rev.*, 2023, **52**, 705–727.
5 G. J. Halder, C. J. Kepert, B. Moubaraki, K. S. Murray and J. D. Cashion, *Science*, 2002, **298**, 1762–1765.
6 J. A. Real, A. B. Gaspar and M. C. Muñoz, *Dalton Trans.*, 2005, 2062–2079.
7 H. L. B. Boström, A. B. Cairns, L. Liu, P. Lazor and I. E. Collings, *Dalton Trans.*, 2020, **49**, 12940–12944.
8 D. Papanikolaou, S. Margadonna, W. Kosaka, S.-i. Ohkoshi, M. Brunelli and K. Prassides, *J. Am. Chem. Soc.*, 2006, **128**, 8358–8363.
9 G. Molnár, L. Salmon, W. Nicolazzi, F. Terki and A. Bousseksou, *J. Mater. Chem. C*, 2014, **2**, 1360–1366.
10 M. D. Manrique-Juárez, S. Rat, L. Salmon, G. Molnár, C. M. Quintero, L. Nicu, H. J. Shepherd and A. Bousseksou, *Coord. Chem. Rev.*, 2016, **308**, 395–408.
11 C. Bartual-Murgui, A. Akou, C. Thibault, G. Molnár, C. Vieu, L. Salmon and A. Bousseksou, *J. Mater. Chem. C*, 2015, **3**, 1277–1285.
12 S. Kamilya, B. Dey, K. Kaushik, S. Shukla, S. Mehta and A. Mondal, *Chem. Mater.*, 2024, **36**, 4889–4915.
13 M. Romanini, Y. X. Wang, K. Gürpinar, G. Ornelas, P. Lloveras, Y. Zhang, W. Zheng, M. Barrio, A. Aznar, A. Gràcia-Condal, B. Emre, O. Atakol, C. Popescu, H. Zhang, Y. Long, L. Balicas, J. L. Tamarit, A. Planes, M. Shatruk and L. Mañosa, *Adv. Mater.*, 2021, **33**, 2008076.
14 K. G. Sandeman, *APL Mater.*, 2016, **4**, 111102.
15 J. Seo, J. D. Braun, V. M. Dev and J. A. Mason, *J. Am. Chem. Soc.*, 2022, **144**, 6493–6503.
16 L. Mañosa and A. Planes, *Adv. Mater.*, 2017, **29**, 1603607.
17 P. Lloveras and J.-L. Tamarit, *MRS Energy Sust.*, 2021, **8**, 3–15.
18 J. Linares, E. Codjovi and Y. Garcia, *Sensors*, 2012, **12**, 4479–4492.
19 L. J. Kershaw Cook, R. Kulmaczewski, R. Mohammed, S. Dudley, S. A. Barrett, M. A. Little, R. J. Deeth and M. A. Halcrow, *Angew. Chem., Int. Ed.*, 2016, **55**, 4327–4331.
20 S. Rodríguez-Jiménez, M. Yang, I. Stewart, A. L. Garden and S. Brooker, *J. Am. Chem. Soc.*, 2017, **139**, 18392–18396.
21 L. T. Birchall, G. Truccolo, L. Jackson and H. J. Shepherd, *Chem. Sci.*, 2022, **13**, 3176–3186.
22 K. Hosoya, T. Kitazawa, M. Takahashi, M. Takeda, J.-F. Meunier, G. Molnár and A. Bousseksou, *Phys. Chem. Chem. Phys.*, 2003, **5**, 1682–1688.
23 K. A. Hofmann and F. Küspert, *Z. Anorg. Chem.*, 1897, **15**, 204–207.
24 J. H. Rayner and H. M. Powell, *J. Chem. Soc.*, 1952, 319–328.
25 T. Kitazawa, T. Kishida, T. Kawasaki and M. Takahashi, *Hyperfine Interact.*, 2017, **238**, 65.
26 P. D. Southon, L. Liu, E. A. Fellows, D. J. Price, G. J. Halder, K. W. Chapman, B. Moubaraki, K. S. Murray, J.-F. Létard and C. J. Kepert, *J. Am. Chem. Soc.*, 2009, **131**, 10998–11009.
27 T. Kitazawa, Y. Gomi, M. Takahashi, M. Takeda, M. Enomoto, A. Miyazaki and T. Enoki, *J. Mater. Chem.*, 1996, **6**, 119–121.
28 Z.-P. Ni, J.-L. Liu, N. Hoque, W. Liu, J.-Y. Li, Y.-C. Chen and M.-L. Tong, *Coord. Chem. Rev.*, 2017, **335**, 28–43.
29 C. Bartual-Murgui, V. Rubio-Giménez, M. Meneses-Sánchez, F. J. Valverde-Muñoz, S. Tatay, C. Martí-Gastaldo, M. C. Muñoz and J. A. Real, *ACS Appl. Mater. Interfaces*, 2020, **12**, 29461–29472.
30 F.-L. Liu and J. Tao, *Chem. – Eur. J.*, 2017, **23**, 18252–18257.
31 A. Orellana-Silla, R. Turo-Cortés, V. Rubio-Giménez, C. Bartual-Murgui, R. Ameloot, C. Martí-Gastaldo, M. C. Muñoz and J. A. Real, *Inorg. Chem. Front.*, 2023, **10**, 600–611.
32 A. A. Lemus-Santana, J. Rodríguez-Hernández, M. González, S. Demeshko, M. Ávila, M. Knobel and E. Reguera, *J. Solid State Chem.*, 2011, **184**, 2124–2130.
33 H. L. B. Boström, *CrystEngComm*, 2020, **22**, 961–968.
34 W.-J. Xu, Z.-Y. Du, W.-X. Zhang and X.-M. Chen, *CrystEngComm*, 2016, **18**, 7915–7928.
35 A. W. Hewat, *Ferroelectrics*, 1973, **6**, 215–218.
36 M. S. Senn, D. A. Keen, T. C. A. Lucas, J. A. Hriljac and A. L. Goodwin, *Phys. Rev. Lett.*, 2016, **116**, 207602.

Open Access Article. Published on 13 June 2025. Downloaded on 1/22/2026 6:47:46 AM. This article is licensed under a Creative Commons Attribution 3.0 Unported Licence.

Open Access Article. Published on 13 June 2025. Downloaded on 1/22/2026 6:47:46 AM. This article is licensed under a Creative Commons Attribution 3.0 Unported Licence.

37 S. C. Miller and W. F. Love, *Tables of Irreducible Representations of Space Groups and Co-Representations of Magnetic Space Groups*, Pruett Press, Boulder, Colorado, 1967.
38 B. J. Campbell, H. T. Stokes, D. E. Tanner and D. M. Hatch, *J. Appl. Crystallogr.*, 2006, **39**, 607–614.
39 C. J. Howard and H. T. Stokes, *Acta Crystallogr., Sect. B: Struct. Sci.*, 1998, **54**, 782–789.
40 J. A. McNulty and P. Lightfoot, *IUCrJ*, 2021, **8**, 485–513.
41 M. V. Talanov, V. B. Shirokov and V. M. Talanov, *Acta Crystallogr., Sect. A: Found. Adv.*, 2016, **72**, 222–235.
42 H. L. B. Boström, M. S. Senn and A. L. Goodwin, *Nat. Commun.*, 2018, **9**, 2380.
43 N. A. Benedek and C. J. Fennie, *Phys. Rev. Lett.*, 2011, **106**, 107204.
44 N. A. Benedek, J. M. Rondinelli, H. Djani, P. Ghosez and P. Lightfoot, *Dalton Trans.*, 2015, **44**, 10543–10558.
45 A. J. Jacobson, J. T. Lewandowski and W. Johnson, *J. Less-Common Met.*, 1986, **116**, 137–146.
46 M. Dion, M. Ganne and M. Tournoux, *Mater. Res. Bull.*, 1981, **16**, 1429–1435.
47 V. Niel, J. M. Martinez-Agudo, M. C. Muñoz, A. B. Gaspar and J. A. Real, *Inorg. Chem.*, 2001, **40**, 3838–3839.
48 C. Bartual-Murgui, N. A. Ortega-Villar, H. J. Shepherd, M. C. Muñoz, L. Salmon, G. Molnár, A. Bousseksou and J. A. Real, *J. Mater. Chem.*, 2011, **21**, 7217–7222.
49 T. Kitazawa, Y. Sato, Y. Gomi, M. Takahashi and M. Takeda, *Mol. Cryst. Liq. Cryst.*, 1996, **286**, 109–114.
50 S. N. Ruddlesden and P. Popper, *Acta Crystallogr.*, 1957, **10**, 538–540.
51 S. Sakaida, K. Otsubo, O. Sakata, C. Song, A. Fujiwara, M. Takata and H. Kitagawa, *Nat. Chem.*, 2016, **8**, 377–383.
52 X.-Y. Hu, X.-L. Cheng, M. Azam, F.-L. Liu and D. Sun, *Inorg. Chem.*, 2024, **63**, 7746–7753.
53 I. A. Gural'skiy, S. I. Shylin, V. Ksenofontov and W. Tremel, *Eur. J. Inorg. Chem.*, 2019, 4532–4537.
54 R. Terrero, Y. Avila, R. Mojica, A. Cano, M. Gonzalez, M. Avila and E. Reguera, *New J. Chem.*, 2022, **46**, 9618–9628.
55 V. García-López, F. Marques-Moros, J. Troya, J. Canet-Ferrer, M. Clemente-León and E. Coronado, *J. Mater. Chem. C*, 2024, **12**, 161–169.
56 R. Turo-Cortés, C. Bartual-Murgui, J. Castells-Gil, M. C. Muñoz, C. Martí-Gastaldo and J. A. Real, *Chem. Sci.*, 2020, **11**, 11224–11234.
57 M. Ahmed, H. E. A. Brand, V. K. Peterson, J. K. Clegg, C. J. Kepert, J. R. Price, B. J. Powell and S. M. Neville, *Dalton Trans.*, 2021, **50**, 1434–1442.
58 R. Ohtani, M. Arai, H. Obha, A. Hori, M. Takata, S. Kitagawa and M. Ohba, *Eur. J. Inorg. Chem.*, 2013, 738–744.
59 D. J. Mondal, N. Mukherjee and S. Konar, *Cryst. Growth Des.*, 2023, **23**, 1832–1839.
60 V. M. Hiiuk, S. Shova, K. V. Domasevitch and I. A. Gural'skiy, *Inorganics*, 2022, **10**, 195.
61 M. Ohba, K. Yoneda, G. Agustí, M. C. Muñoz, A. B. Gaspar, J. A. Real, M. Yamasaki, H. Ando, Y. Nakao, S. Sakaki and S. Kitagawa, *Angew. Chem., Int. Ed.*, 2009, **48**, 4767–4771.
62 A. M. Glazer, *Acta Crystallogr., Sect. B: Struct. Crystallogr. Cryst. Chem.*, 1972, **28**, 3384–3392.
63 M. W. Lufaso, R. B. Macquart, Y. Lee, T. Vogt and H.-C. zur Loye, *J. Solid State Chem.*, 2006, **179**, 917–922.
64 M. L. Medarde, *J. Phys.: Condens. Matter*, 1997, **9**, 1679–1707.
65 S. G. Duyker, J. A. Hill, C. J. Howard and A. L. Goodwin, *J. Am. Chem. Soc.*, 2016, **138**, 11121–11123.
66 H. L. B. Boström and W. R. Brant, *J. Mater. Chem. C*, 2022, **10**, 13690–13699.
67 M. González, A. Lemus-Santana, J. Rodríguez-Hernández, M. Knobel and E. Reguera, *J. Solid State Chem.*, 2013, **197**, 317–322.
68 T. Kosone, R. Kosuge, M. Tanaka, T. Kawasaki and N. Adachi, *New J. Chem.*, 2022, **46**, 10540–10544.
69 D. J. Mondal, A. Mondal, A. Paul and S. Konar, *Inorg. Chem.*, 2022, **61**, 4572–4580.
70 V. Martínez, A. B. Gaspar, M. C. Muñoz, G. V. Bukin, G. Levchenko and J. A. Real, *Chem. Eur. J.*, 2009, **15**, 10960–10971.
71 F. J. Valverde-Muñoz, M. Seredyuk, M. C. Muñoz, K. Znovjyak, I. O. Fritsky and J. A. Real, *Inorg. Chem.*, 2016, **55**, 10654–10665.
72 H. L. B. Boström, J. A. Hill and A. L. Goodwin, *Phys. Chem. Chem. Phys.*, 2016, **18**, 31881–31894.
73 A. Martinez-Martinez, E. Resines-Urien, N. S. Settineri, S. J. Teat, E. C. Sañudo, O. Fabelo, J. A. Rodriguez-Velamazan, L. Piñeiro-López and J. S. Costa, *Cryst. Growth Des.*, 2023, **23**, 3952–3957.
74 L. Piñeiro-López, M. Seredyuk, M. C. Muñoz and J. A. Real, *Eur. J. Inorg. Chem.*, 2020, 764–769.
75 L. Piñeiro-López, F. J. Valverde-Muñoz, M. Seredyuk, M. C. Muñoz, M. Haukka and J. A. Real, *Inorg. Chem.*, 2017, **56**, 7038–7047.
76 M. Ahmed, K. A. Zenere, N. F. Sciortino, K. S. A. Arachchige, G. F. Turner, J. Cruddas, C. Hua, J. R. Price, J. K. Clegg, F. J. Valverde-Muñoz, J. A. Real, G. Chastanet, S. A. Moggach, C. J. Kepert, B. J. Powell and S. M. Neville, *Inorg. Chem.*, 2022, **61**, 6641–6649.
77 N.-T. Yao, L. Zhao, H.-Y. Sun, C. Yi, Y.-H. Guan, Y.-M. Li, H. Oshio, Y.-S. Meng and T. Liu, *Angew. Chem., Int. Ed.*, 2022, **61**, e202208208.
78 B. L. Matthews, N. C. Harvey-Reid, E. Jangodaz, V.-J. Scott, M. I. J. Polson, A. Maibam, R. Babarao, S. G. Telfer and P. E. Kruger, *J. Mater. Chem. A*, 2024, **12**, 15106–15114.
79 I. S. Kuzevanova, O. I. Kucheriv, V. M. Hiiuk, D. D. Naumova, S. Shova, S. I. Shylin, V. O. Kotsyubynsky, A. Rotaru, I. O. Fritsky and I. A. Gural'skiy, *Dalton Trans.*, 2021, **50**, 9250–9258.
80 R. Turo-Cortés, F. J. Valverde-Muñoz, M. Meneses-Sánchez, M. C. Muñoz, C. Bartual-Murgui and J. A. Real, *Inorg. Chem.*, 2021, **60**, 9040–9049.
81 P. Gütlich, *Eur. J. Inorg. Chem.*, 2013, 581–591.

 This journal is © The Royal Society of Chemistry 2025

Open Access Article. Published on 13 June 2025. Downloaded on 1/22/2026 6:47:46 AM.
This article is licensed under a Creative Commons Attribution 3.0 Unported Licence.

82 M. J. Pitcher, P. Mandal, M. S. Dyer, J. Alaria, P. Borisov, H. Niu, J. B. Claridge and M. J. Rosseinsky, *Science*, 2015, **347**, 420–424.
83 Z. Feng, J.-J. Ling, H. Song and D. Zhu, *Inorg. Chem. Front.*, 2023, **10**, 305–315.
84 N. F. Sciortino, K. R. Scherl-Gruenwald, G. Chastanet, G. J. Halder, K. W. Chapman, J.-F. Létard and C. J. Kepert, *Angew. Chem., Int. Ed.*, 2012, **51**, 10154–10158.
85 C.-F. Wang, J. C. Wu and Q. Li, *Inorg. Chem. Front.*, 2022, **9**, 3251–3258.
86 M. Ahmed, K. S. A. Arachchige, Z. Xie, J. R. Price, J. Cruddas, J. K. Clegg, B. J. Powell, C. J. Kepert and S. M. Neville, *Inorg. Chem.*, 2022, **61**, 11667–111674.
87 M. Meneses-Sánchez, R. Turo-Cortés, C. Bartual-Murgui, I. da Silva, M. C. Muñoz and J. A. Real, *Inorg. Chem.*, 2021, **60**, 11866–11877.
88 M. J. Cliffe, E. N. Keyzer, M. T. Dunstan, S. Ahmad, M. F. L. De Volder, F. Deschler, A. J. Morris and C. P. Grey, *Chem. Sci.*, 2019, **10**, 793–801.
89 M. Seredyuk, A. B. Gaspar, V. Ksenofontov, M. Verdaguer, F. Villain and P. Gütlich, *Inorg. Chem.*, 2009, **48**, 6130–6141.
90 A. M. Davenport, C. R. Marshall, T. Nishiguchi, K. Kadota, A. B. Andreeva, S. Horike and C. K. Brozek, *J. Am. Chem. Soc.*, 2024, **146**, 23692–23698.
91 R. Ohtani and S. Hayami, *Chem. – Eur. J.*, 2017, **23**, 2236–2248.
92 S. Brooker, *Chem. Soc. Rev.*, 2015, **44**, 2880–2892.
93 S. Dissegna, K. Epp, W. R. Heinz, G. Kieslich and R. A. Fischer, *Adv. Mater.*, 2018, 1704501.
94 C. Bartual-Murgui, A. Akou, H. J. Shepherd, G. Molnár, J. A. Real, L. Salmon and A. Bousseksou, *Chem. Eur. J.*, 2013, **19**, 15036–15043.
95 T. Kitazawa, M. Eguchi and M. Takeda, *Mol. Cryst. Liq. Cryst.*, 2000, **341**, 527–532.
96 J. Okabayashi, S. Ueno, Y. Wakisaka and T. Kitazawa, *Inorg. Chim. Acta*, 2015, **426**, 142–145.
97 D. A. Keen and A. L. Goodwin, *Nature*, 2015, **521**, 303–309.
98 G. Agustí, R. Ohtani, K. Yoneda, A. B. Gaspar, M. Ohba, J. F. Sánchez-Royo, M. C. Muñoz, S. Kitagawa and J. A. Real, *Angew. Chem.*, 2009, **121**, 9106–9109.
99 R. Ohtani, K. Yoneda, S. Furukawa, H. Horike, S. Kitagawa, A. B. Gaspar, M. C. Muñoz, J. A. Real and M. Ohba, *J. Am. Chem. Soc.*, 2011, **133**, 8600–8605.
100 J. P. Janet, L. Chan and H. J. Kulik, *J. Phys. Chem. Lett.*, 2018, **9**, 1064–1071.
101 V. Vennelakanti, I. B. Kilic, G. G. Terrones, C. Duan and H. J. Kulik, *J. Phys. Chem. A*, 2024, **128**, 204–216.
102 K. Morita, D. W. Davies, K. T. Butler and A. Walsh, *Chem. Mater.*, 2022, **34**, 562–573.